Paper I:
Intermittent fluctuations due to Lorentzian pulses in turbulent thermal convection

G. Decristoforo ⬛, A. Theodorsen ⬛, and O. E. Garcia ⬛

View Online   Export Citation   CrossMark

Intermittent fluctuations due to Lorentzian pulses in turbulent thermal convection

View Online   Export Citation   CrossMark

G. Decristoforo,[a] (ID) A. Theodorsen,[b] (ID) and O. E. Garcia[c] (ID)

AFFILIATIONS

Department of Physics and Technology, UiT The Arctic University of Norway, NO-9037 Tromsø, Norway

[a] Author to whom correspondence should be addressed: gregor.decristoforo@uit.no
[b] audun.theodorsen@uit.no
[c] odd.erik.garcia@uit.no

ABSTRACT

Turbulent motions due to flux-driven thermal convection are investigated by numerical simulations and stochastic modeling. Tilting of convection cells leads to the formation of sheared flows and quasi-periodic relaxation oscillations for the energy integrals far from the threshold for linear instability. The probability density function for the temperature and radial velocity fluctuations in the fluid layer changes from a normal distribution at the onset of turbulence to a distribution with an exponential tail for large fluctuation amplitudes for strongly driven systems. The frequency power spectral density has an exponential shape, which is a signature of deterministic chaos. By use of a novel deconvolution method, this is shown to result from the presence of Lorentzian pulses in the underlying time series, demonstrating that exponential frequency spectra can also persist in turbulent flow regimes.

Published under license by AIP Publishing. https://doi.org/10.1063/5.0012017

I. INTRODUCTION

Buoyancy-driven motion of a fluid confined between horizontal plates is a cornerstone of fluid mechanics and has many areas of application, including astrophysics, industry, laboratory fluid dynamics, meteorology, oceanography, and plasma physics. Due to its rich dynamics, the Rayleigh–Bénard convection model has become a paradigm to investigate pattern formation, nonlinear phenomena, and scaling relationships.[1–6]

For sufficiently strong forcing, oscillating fluid motion, and chaotic behavior results. An intrinsic property of deterministic chaos is an exponential frequency power spectral density for the fluctuations. This has been observed in numerous experiments and model simulations of fluids and magnetized plasmas.[7–27] Recently, the exponential spectrum has been attributed to the presence of uncorrelated Lorentzian pulses in the temporal dynamics.[29–43] This includes the Lorenz model, which describes chaotic dynamics in Rayleigh–Bénard convection.[23–30]

In two-dimensional thermal convection, it is well known that the convection rolls in a horizontally periodic domain can give rise to the spontaneous formation of strong mean flows through a tilting instability.[44–63] For strongly driven thermal convection,

turbulent states develop where the sheared mean flows transiently suppress the fluctuating motions, resulting in quasi-periodic relaxation oscillations.[57–74] Similar relaxation oscillations have also been identified in turbulent plasmas.[75–86] This dynamics has been described in terms of a predator–prey system, with a conservative transfer of kinetic energy from the fluctuating to the mean motions and a viscous dissipation of the latter.[60–63,87–90] The velocity and temperature fluctuations throughout the fluid layer are strongly intermittent with positive skewness and flatness moments. The probability density functions have exponential tails, resembling the state of hard turbulence in Rayleigh–Bénard convection.[91–100]

In this contribution, it is for the first time demonstrated that these properties of irregular fluid motion can be present simultaneously. The fluctuation statistics in a state of turbulent convection are investigated by numerical simulations of a fluid layer driven by a fixed heat flux.[60,101–103] Time-series analysis and stochastic modeling of the temperature field are presented. It is demonstrated that the frequency power spectral density of the fluctuations has an exponential tail. A novel deconvolution algorithm is applied, showing that the temperature signal can be described as a superposition of Lorentzian pulses. Hence, the well-known properties of deterministic chaos can persist even in turbulent flow regimes.

The outline of this paper is as follows: In Sec. II, we present the model equations and briefly discuss the shear flow generation mechanism. In Sec. III, the basic results from the numerical simulations are presented. The fluctuation statistics are presented in Sec. IV and in Sec. V; it is demonstrated that the exponential frequency power spectral density is due to the presence of Lorentzian pulses in the time series. The conclusions and a summary of the results are presented in Sec. VI. The Appendix presents a derivation of the frequency power spectral density due to a periodic train of pulses with fixed shape and duration.

II. MODEL EQUATIONS

Considering two-dimensional fluid motions in a gravitational field opposite to the x-axis, the model equations describing thermal convection are given by

$$\left(\frac{\partial}{\partial t} + \widehat{\mathbf{z}} \times \nabla \psi \cdot \nabla\right)\Theta = \kappa \nabla^2 \Theta, \tag{1a}$$

$$\left(\frac{\partial}{\partial t} + \widehat{\mathbf{z}} \times \nabla \psi \cdot \nabla\right)\Omega + \frac{\partial \Theta}{\partial y} = \mu \nabla^2 \Omega, \tag{1b}$$

where Θ describes the temperature, ψ is the stream function for the two-dimensional fluid velocity field $\mathbf{v} = \widehat{\mathbf{z}} \times \nabla \psi$, and $\Omega = \widehat{\mathbf{z}} \cdot \nabla \times \mathbf{v} = \nabla^2 \psi$ is the associated fluid vorticity. The temperature perturbations are normalized by the temperature difference $\triangle T$ over the fluid layer in hydrostatic equilibrium, length scales are normalized by the fluid layer depth d, and time is normalized by the ideal interchange rate.[101–103] The normalized heat diffusivity κ and viscosity μ are related to the Rayleigh and Prandtl numbers by $R = 1/\kappa\mu$ and $P = \mu/\kappa$, respectively. The temperature in hydrostatic equilibrium is given by $\Theta = 1 - x$. A similar mathematical model also describes fluctuations in non-uniformly magnetized plasmas where the symmetry axis z corresponds to the direction of the magnetic field and the effective gravity is due to magnetic field curvature.[50–54,57–63]

In many cases, the fluid is confined in a geometry where x corresponds to the radial coordinate and y the azimuthal direction. In the following, we therefore refer to the x- and y-direction as radial and azimuthal, respectively. All dependent variables are accordingly assumed to be periodic in the azimuthal direction, for example, $\Theta(y) = \Theta(y + L)$. In the radial direction, the boundary conditions are taken to be

$$\psi(x = 0) = \psi(x = 1) = 0, \tag{2a}$$

$$\Omega(x = 0) = \Omega(x = 1) = 0, \tag{2b}$$

$$\frac{\partial \Theta}{\partial x}(x = 0) = -1, \quad \Theta(x = 1) = 0. \tag{2c}$$

The latter condition corresponds to a fixed conductive heat flux through the fluid layer.[60,101–103] It should be noted that the free-slip boundary conditions imply that there is no convective heat transport through the radial boundaries since $v_x = -\partial\psi/\partial y = 0$ for $x = 0, 1$.

For the azimuthally periodic system, it is convenient to define the profile of any dependent variable as its azimuthal average and denote this by a zero subscript. For the temperature field Θ, this is given by

$$\Theta_0(x, t) = \frac{1}{L}\int_0^L dy\, \Theta(\mathbf{x}, t). \tag{3}$$

The motivation for separating profiles and spatial fluctuations is simply that the latter are the components mediating the radial convective heat flux, while the former describes the modifications of the equilibrium state profiles.

Similar to the temperature profile, an average azimuthal flow is also defined by

$$v_0(x, t) = \frac{1}{L}\int_0^L dy\, \frac{\partial \psi}{\partial x} = \frac{\partial \psi_0}{\partial x}. \tag{4}$$

Due to the conservation of net circulation of the fluid layer, the mean azimuthal flow is intrinsically sheared and corresponds to differential rotation of the fluid layer. Such flows develop due to a tilting instability of the convective cells.[44–63] Since the symmetric flow v_0 is intrinsically incapable of mediating radial convective transport, it is natural to separate the kinetic energy into two components comprised by the fluctuating motions and the sheared mean flows, defined, respectively, by

$$K(t) = \int d\mathbf{x}\, \frac{1}{2}\left[\nabla(\psi - \psi_0)\right]^2, \qquad U(t) = \int d\mathbf{x}\, \frac{1}{2}\, v_0^2. \tag{5}$$

The evolution of these energy integrals are readily derived from the mean vorticity equation,[60–63]

$$\frac{dK}{dt} = \int d\mathbf{x}\, v_x \Theta - \Pi - \mu \int d\mathbf{x}\, (\Omega - \Omega_0)^2, \tag{6}$$

$$\frac{dU}{dt} = \Pi - \mu \int d\mathbf{x}\, \Omega_0^2, \tag{7}$$

where the kinetic energy transfer rate from the fluctuating motions to the sheared mean flows is defined by

$$\Pi = \int d\mathbf{x}\, v_0 \frac{\partial}{\partial x}(v_x v_y). \tag{8}$$

As expected, the convective transport drive for the kinetic energy integral in Eq. (6) appears only for the fluctuating motions, while viscous dissipation damps kinetic energy in either form. The radial convective transport of azimuthal momentum evidently yields a conservative transfer of kinetic energy between the fluctuating motions and the azimuthally mean flows.

Numerical simulations have shown that turbulent convection can display predator–prey-like relaxation oscillations for the energy integrals,[57–62] which can be interpreted as follows: Initially, the convective energy grows exponentially due to the primary instability. When the fluctuation level becomes sufficiently large to sustain the sheared mean flows against viscous dissipation, this flow energy grows at the expense of the convective motions. The spatial fluctuations are effectively stabilized at a sufficiently strong shear flow. Kinetic energy is, however, continuously transferred to the mean flows, leading to an almost complete suppression of the fluctuation energy and, thus, the radial convective transport. Subsequently, there are no fluctuating motions to sustain the sheared flows, which hence decay on a viscous time scale. Finally, as the mean flows become sufficiently weak, the convective energy again starts to grow and the cycle repeats. As will be seen from the numerical simulations presented in Sec. III, this leads to a strong modulation of the fluctuations.

III. TURBULENT CONVECTION

The temperature and vorticity equations are solved numerically by combining a finite difference and a Fourier–Galerkin method for spatial discretization using an Arakawa scheme for the exact conservation of energy and enstrophy. The resolution of the simulation domain is set to 128×128 grid points. For time discretization, a third order stiffly stable integrator is used[83,104,105] with a time step of $\Delta t = 5 \times 10^{-3}$. Time series of the dependent variables are recorded at radially equidistant points in the simulation domain and analyzed in the following.

For sufficiently high Rayleigh numbers, numerical simulations of the two-dimensional thermal convection model result in turbulent states.[60–62] Previously, it has been shown that close to the onset of turbulent convection, for $R = 4 \times 10^5$ and $P = 1$, the radial velocity fluctuations in the center of the domain are normally distributed.[60] Increasing the Rayleigh number to $R = 2 \times 10^6$ results in a probability distribution function for the radial velocity fluctuations with exponential tails.[60–62] Previous investigations have shown that the large-amplitude fluctuations are associated with coherent structures propagating through the fluid layer. Here, we present a detailed analysis of the fluctuation statistics in the latter parameter regime (with $R = 2 \times 10^6$, $P = 1$, corresponding to $\kappa = \mu = 7.07 \times 10^{-4}$ and $L = L_x = L_y = 1$), resembling the state of hard turbulence in thermal convection experiments.[91–100]

The time-averaged profile of the temperature and the relative fluctuation level are presented in Fig. 1. Here and in the following, angular brackets indicate a time average. The turbulent motions significantly reduce the heat confinement in the fluid layer, reducing the temperature on the left boundary from unity in the case of only heat conduction to less than 0.343 on average in the turbulent state. There is a significant profile gradient in the center of the fluid layer. The relative fluctuation level increases drastically from the center of the domain and radially outward, reaching more than 0.5 close to the outer boundary.

The intermittency of the fluctuations is quantified by the skewness moment, defined by $S_\Theta = \langle (\Theta - \langle \Theta \rangle)^3 \rangle / \Theta_{rms}^3$, and the flatness moment, defined by $F_\Theta = \langle (\Theta - \langle \Theta \rangle)^4 \rangle / \Theta_{rms}^4 - 3$, where the variance is given by $\Theta_{rms}^2 = \langle (\Theta - \langle \Theta \rangle)^2 \rangle$. Both the skewness and flatness moments vanish for a normally distributed random variable. The profile of these moments for the temperature fluctuations is presented in Fig. 2. This shows that the probability density for the fluctuations is positively skewed and flattened in the outer part
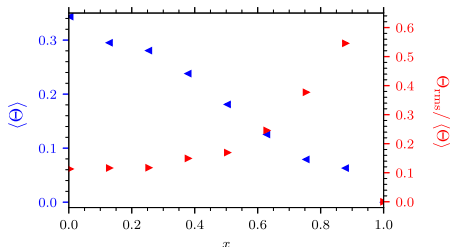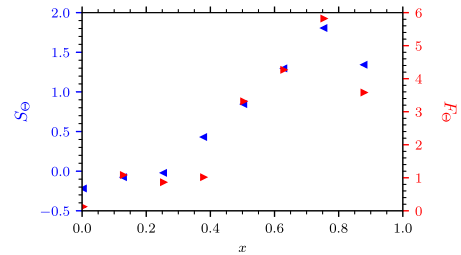

FIG. 2. Time-averaged profile of the skewness and flatness moments for the temperature fluctuations.

of the simulation domain, suggesting frequent appearance of large-amplitude bursts in the time series at a fixed point in the fluid layer. The moments are largest at $x = 3/4$, where the skewness is 1.81, while the flatness moment is 5.82. This demonstrates a strong departure from a normal distribution of the fluctuations.

The time-averaged profile of the stream function is presented in Fig. 3 together with the root mean square fluctuation level of the radial velocity. The time-averaged stream function has a near half-period sinoidal variation over the fluid layer and vanishes at the boundaries. This implies an average counter-streaming mean flow in the fluid layer, which vanishes in the center of the domain and is strongest close to the boundaries. However, the radial velocity fluctuation vanishes at the boundaries due to the stress-free boundary conditions. The velocity fluctuation level has a local minimum in the center of the domain. At $x = 3/4$, the mean flow is 0.155, resulting in a vertical transit time of ~ 6.46 in non-dimensional units. There are some changes in this transit time since the mean flow velocity changes in time, as discussed later.

The evolution of the kinetic energy in the fluctuating and mean motions for a short part of the simulation run is presented in Fig. 4. This shows the quasi-periodic relaxation oscillations resembling predator–prey type dynamics, where kinetic energy is transferred from the fluctuating motions to the sheared flows and subsequently dissipated by viscosity. The auto-correlation function for the energy integrals is presented in Fig. 5. The mean flow energy

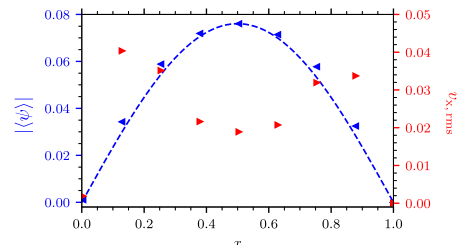FIG. 1. Time-averaged profile of the temperature and the relative fluctuation level.

FIG. 3. Time-averaged profile of the stream function and the root mean square value of the radial velocity. The dashed line shows a half-period sine function fit to the stream function profile.
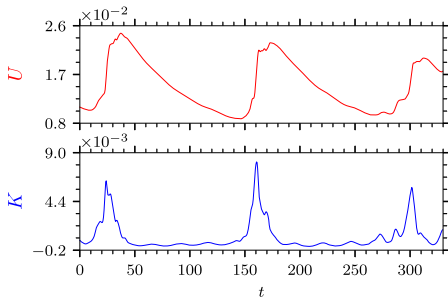
FIG. 4. Evolution of the kinetic energy in fluctuating, K, and mean flows, U, showing predator–prey-like relaxation oscillations.
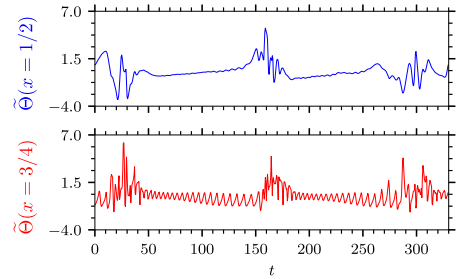

FIG. 6. Time series of the temperature fluctuations at $x = 1/2$ and $x = 3/4$.

auto-correlation function has a damped oscillatory behavior with a period of ~125, corresponding to the characteristic separation between bursts in the energy integrals. The auto-correlation function for the energy in the fluctuating motions has a decay time of ~25, which is attributed to the characteristic duration of the bursts in the kinetic energy seen in Fig. 4. This has been confirmed by conditional averaging of large-amplitude events in the energy integral time series.

In Fig. 6, the normalized temperature fluctuations $\widetilde{\Theta} = (\Theta - \langle\Theta\rangle)/\Theta_{\mathrm{rms}}$ recorded in the center of the fluid layer, at $x = 1/2$, and in the outer part, at $x = 3/4$, are presented. The evolution of the temperature during the onset of a turbulent period is shown in Fig. 7. This shows the presence of a structure moving radially through the fluid layer as well as azimuthally due to a sheared mean flow. Throughout the fluid layer, the fluctuations are strongly intermittent with large bursts during the time of strong activity in the energy of the fluctuating motions presented in Fig. 4. In the outer part of the fluid layer, the fluctuations have a nearly periodic oscillation in the periods between the bursts in the energy integrals. This is due to the sheared mean flow with a transit time of ~6.46. In the following, the statistical properties of these fluctuations will be elucidated.
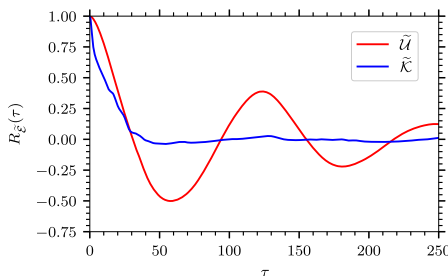

FIG. 5. Auto-correlation function for the kinetic energy in fluctuating and mean flows.

IV. FLUCTUATION STATISTICS

The probability density function for the temperature fluctuations measured at $x = 1/2$ and $x = 3/4$ is presented in Fig. 8. As expected from the radial variation of the skewness and kurtosis moments, the distributions have elevated tails compared to a normal distribution. For $x = 3/4$, the distribution is strongly skewed and has a nearly exponential tail toward large values. This is demonstrated by the solid line in Fig. 8, which is the best fit of a convolution of a normal distribution and a Gamma distribution. Similarly, the probability distribution functions for the radial velocity fluctuations are presented in Fig. 9 together with the best fit of a convolution between a Laplace and a normal distribution. This clearly demonstrates the presence of exponential tails in the probability densities.

The frequency power spectral densities for the temperature signals measured at $x = 1/2$ and $x = 3/4$ are presented in semi-logarithmic plots in Figs. 10 and 11. From Fig. 10, with logarithmic scaling of the frequency, it is clear that the frequency spectrum has a pronounced maximum at the linear frequency $f = 8 \times 10^{-3}$, which corresponds to the characteristic time between bursts in the energy integrals discussed above. Some higher harmonics of this frequency peak are also readily identified. The frequency spectrum for $x = 3/4$ also has a peak at $\sim f = 0.2$, corresponding to the vertical transit time by the average mean flow.

When the spectra are plotted with a logarithmic scaling for the power as presented in Fig. 11, it is clearly seen that frequency power spectral density has an exponential decay on the form $\exp(-4\pi\tau_{\mathrm{d}}|f|)$, with the characteristic time $\tau_{\mathrm{d}} = 0.637$ for $x = 1/2$ and $\tau_{\mathrm{d}} = 0.382$ for $x = 3/4$. In Sec. V, it will be demonstrated that the exponential spectrum is due to the presence of Lorentzian pulses in the time series and that the slope corresponds to the duration time of these pulses. Similar exponential frequency spectra are also found for the stream function, radial velocity, and vorticity field. However, the slope, and therefore the duration time of the underlying pulses, varies for the different quantities.

V. LORENTZIAN PULSES

An exponential frequency power spectrum is a signature of deterministic chaos and has been attributed to Lorentzian-shaped pulses in the underlying time series. In order to demonstrate this, consider the stochastic process that gives a superposition of pulses
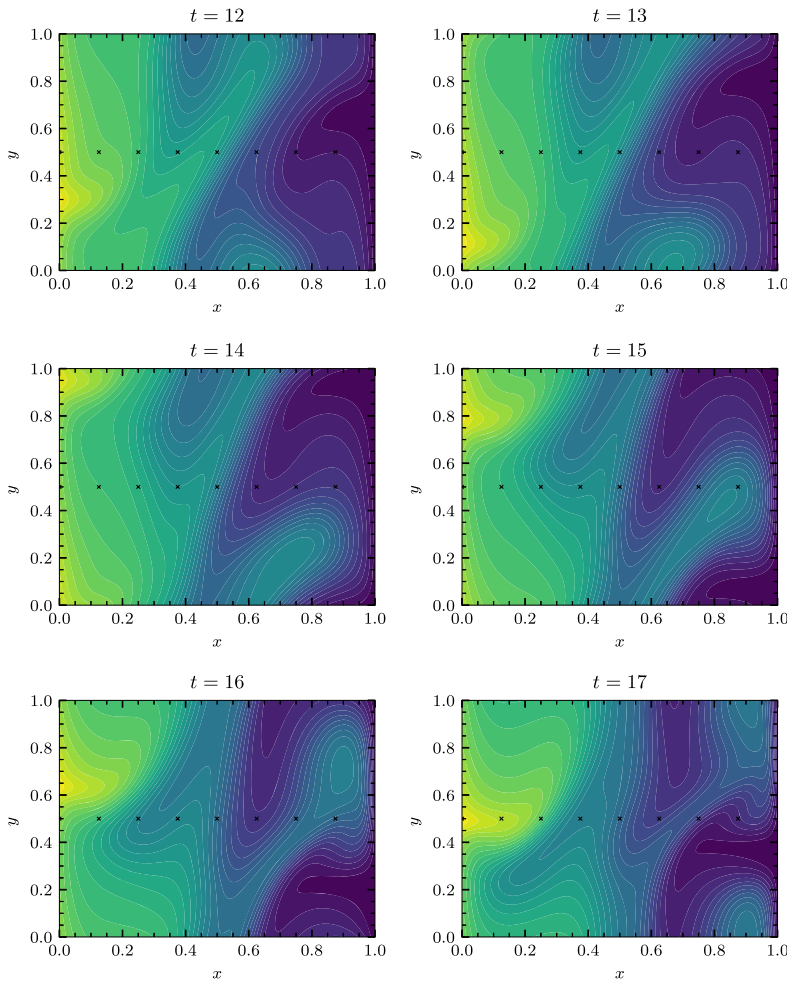
FIG. 7. Exemplary snapshots of the temperature field Θ, showing the evolution at the onset of a turbulent period. The black crosses show the radially equidistant positions where time series are recorded.

with fixed shape ϕ and duration τ_d,[106–117]

$$\Phi_K(t) = \sum_{k=1}^{K(T)} A_k \phi\left(\frac{t - t_k}{\tau_d}\right), \qquad (9)$$

where A_k and t_k are pulse amplitude and arrival time for the pulse labeled k, respectively, and $K(T)$ is the number of pulses present in a time interval of duration T. In the case of Lorentzian pulses, the function ϕ is given by[39–41]

$$\phi(\theta) = \frac{1}{\pi} \frac{1}{1 + \theta^2}. \qquad (10)$$

In the case of uncorrelated Lorentzian pulses, it was recently shown that the frequency power spectral density is exponential, and for the normalized variable $\widetilde{\Phi} = (\Phi - \langle\Phi\rangle)/\Phi_{rms}$, it is given by[39,40]

$$\mathscr{S}_{\widetilde{\Phi}}(f) = 2\pi\tau_d \exp(-4\pi\tau_d|f|).$$

In the Appendix, it is shown that for a periodic sequence of Lorentzian pulses with fixed duration, the frequency power spectrum is a product of the exponential spectrum and a uniform delta pulse train at frequencies corresponding to multiples of the inverse periodicity time. In the case of a slight irregularity in the period between the pulses, the delta peaks in the frequency spectrum with broaden and have finite amplitude.
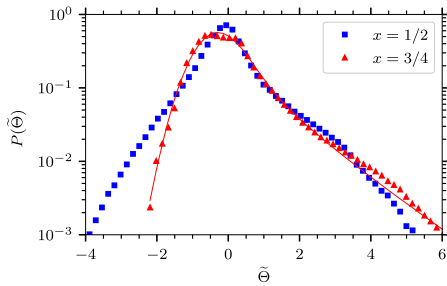
FIG. 8. Probability density function for the normalized temperature fluctuations at $x = 1/2$ and $x = 3/4$. The solid line shows the best fit of a convolution between a Gamma and a normal distribution.
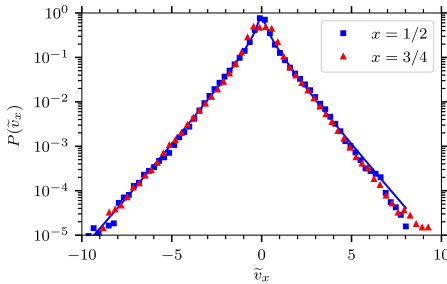

FIG. 11. Frequency power spectral density for temperature fluctuations at $x = 1/2$ and $x = 3/4$. The dashed lines show the best fit of an exponential function.

FIG. 9. Probability density function for the normalized radial velocity fluctuations at $x = 1/2$ and $x = 3/4$. The solid line shows the best fit of a convolution between a Laplace and a normal distribution.

As shown in Fig. 6, the temperature time series at $x = 3/4$ can be separated into parts with nearly periodic oscillations and turbulent parts with chaotic, large-amplitude fluctuations. An example of separating these periods is shown in Fig. 12. In Fig. 13, the frequency power spectral density of the quasi-periodic and turbulent parts is
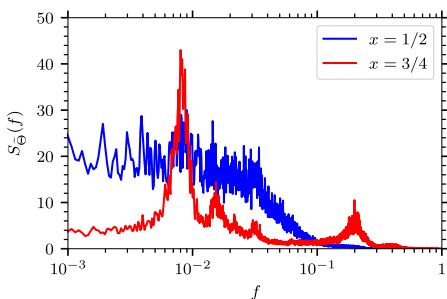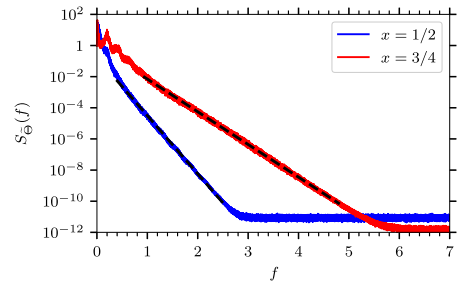
shown together with the power spectral density of the entire signal. It is clear that the power spectrum of the entire signal is well described by the power spectrum of the turbulent parts and that they have the same time scale, $\tau_d = 0.382$. The black dashed line gives an exponential spectrum with 4 times the duration time of the whole spectrum, which closely resembles the power spectrum of the quasi-periodic parts of the signal. In the following, this is used as an estimated duration time of the periodic part.

In order to demonstrate that the temperature time series can be described as a superposition of Lorentzian pulses, a deconvolution algorithm using a Lorentzian pulse with fixed duration time estimated from the power spectral density is applied. This gives the pulse amplitudes and arrival times, which can be used to reconstruct the original signal. The superposition of pulses with fixed duration given by Eq. (9) can be written as a convolution between the pulse function and a train of delta pulses,[114,118]

$$\Phi_K(t) = [\phi * F_K]\left(\frac{t}{\tau_d}\right), \tag{11}$$

where

$$F_K(t) = \sum_{k=1}^{K(T)} A_k \delta\left(\frac{t - t_k}{\tau_d}\right). \tag{12}$$

FIG. 10. Logarithm of the frequency power spectral density for temperature fluctuations at $x = 1/2$ and $x = 3/4$.
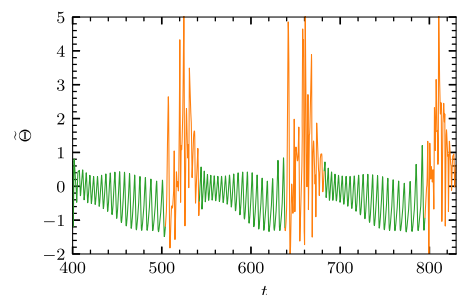

FIG. 12. Example of splitting of temperature fluctuations into quasi-periodic (green) and turbulent (orange) parts at $x = 3/4$.
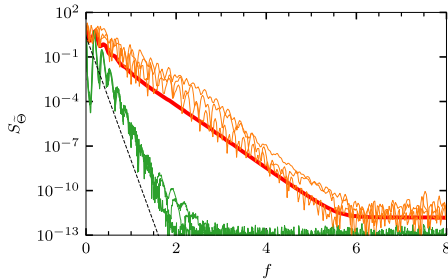
FIG. 13. Power spectral density of the temperature fluctuations at $x = 3/4$. The red line gives the spectrum of the entire time series as shown in Fig. 10, the orange lines give the spectra of the turbulent parts from Fig. 12, while the green lines give the spectra of the quasi-periodic parts. The black dashed line gives the prediction for an exponential spectrum with the periodicity time seen in the raw time series.
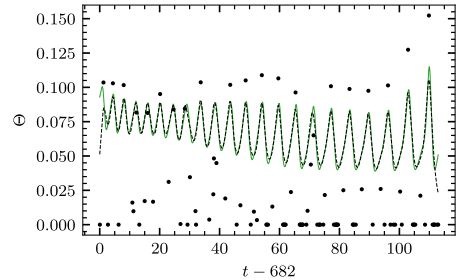

FIG. 15. Excerpt of quasi-periodic part (green solid line) and reconstructed signal from the deconvolution (black dashed line). The dots indicate arrival times and amplitudes of Lorentzian pulses with duration time $\tau_d = 1.528$. The circular dots give half the true amplitude value for better comparison with the time series.

The goal is to find the forcing $F_K(t)$ and to estimate the pulse amplitudes $\{A_k\}_{k=1}^{K}$ and arrival times $\{t_k\}_{k=1}^{K}$ as accurately as possible. In order to do this, a modified version of the Richardson–Lucy deconvolution algorithm will be used.[118–123] Following this scheme, an initial guess for F_K is made, denoted by $F_K^{(1)}$. The numerical value of this initial forcing matters little and can be set as some positive constant or the signal itself. The initial value is updated iteratively, with the nth iteration given by

$$F_K^{(n+1)} = F_K^{(n)} \frac{D * \widehat{\phi}}{F_K^{(n)} * \phi * \widehat{\phi}}, \tag{13}$$

where $\widehat{\phi}(t) = \phi(-t)$. Here and in the following, D denotes any of the simulation data time series discussed above.

The result from the deconvolution algorithm is presented in Figs. 14 and 15 for representative turbulent and the quasi-periodic parts, respectively. It is clear that most of the signals are well reconstructed by a superposition of Lorentzian pulses. As an example,
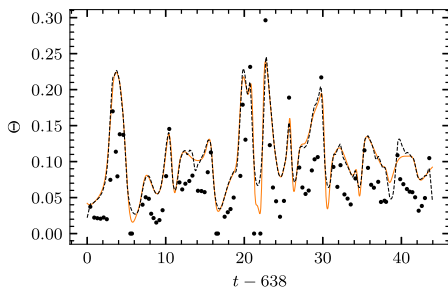
the first peak in Fig. 14 results from a structure of high temperature moving radially through the fluid layer similar to the structures shown in Fig. 7. The lift-time of the two-dimensional structure in Fig. 7 exceeds the duration of the Lorentzian-shaped peak in Fig. 14, but the single-point recording can be modeled as a compound of several Lorentzian pulses. The frequency power spectral density of the reconstructed time series accurately reproduces that from the numerical simulations as expected. This analysis clearly demonstrates that the exponential frequency spectra for the temperature fluctuations in the thermal convection simulations are due to the presence of Lorentzian pulses in the time series.

VI. DISCUSSION AND CONCLUSIONS

In this contribution, the statistical properties of the temperature fluctuations in numerical simulations of turbulent thermal convection have been investigated by time-series analysis and stochastic modeling. The generation of a sheared mean flow through the fluid layer results in predator–prey-like dynamics of the energy integrals and leads to multiple temporal scales in the dynamics. For sufficiently large Rayleigh numbers, a regime corresponding to hard turbulence results with exponential tails in the probability distribution function for the temperature and velocity fluctuations.

The frequency power spectral density for the fluctuations has local maxima at frequencies corresponding to bursting in the energy integral as well as transit time for the mean flow through the fluid layer. However, when presented in a semi-logarithmic plot, it is clear that the frequency spectrum has an exponential tail for power densities all the way down to round off errors. A novel deconvolution method has been used to show that the exponential spectrum is due to the presence of Lorentzian pulses in the temperature time series. The time scale for the structures is consistent with the slope of the exponential frequency spectra.

FIG. 14. Excerpt of turbulent part (orange solid line) and reconstructed signal from the deconvolution (black dashed line). The dots indicate arrival times and amplitudes of Lorentzian pulses with duration time $\tau_d = 0.382$. The circular dots give half the true amplitude value for better comparison with the time series.

APPENDIX: PERIODIC ARRIVALS

In this appendix, the frequency power spectral density for a superposition of pulses with periodic arrivals is calculated. A superposition of K pulses with fixed shape and duration, as given by Eq. (9), can be written as a convolution between the pulse function ϕ and a train of delta pulses,

$$\Phi_K(t) = \int_{-\infty}^{\infty} \mathrm{d}\theta \, \phi\left(\frac{t}{\tau_\mathrm{d}} - \theta\right) F_K(\theta), \qquad (A1)$$

where the forcing F_K due to the delta pulse train is given by

$$F_K(\theta) = \sum_{k=1}^{K} A_k \delta\left(\theta - \frac{t_k}{\tau_\mathrm{d}}\right). \qquad (A2)$$

The pulse duration time τ_d is taken to be the same for all pulses, and the pulse amplitudes A_k are taken to be randomly distributed with mean value $\langle A \rangle$ and variance $A_\mathrm{rms}^2 = \langle (A - \langle A \rangle)^2 \rangle$. The pulse function is assumed to be localized and normalized such that[112,115]

$$\int_{-\infty}^{\infty} \mathrm{d}\theta \, |\phi(\theta)| = 1.$$

The frequency power spectral density of a random process $\Phi_K(t)$ is defined as

$$\mathscr{S}_\Phi(\omega) = \lim_{T \to \infty} \langle |\mathscr{F}_T[\Phi_K](\omega)|^2 \rangle, \qquad (A3)$$

where the Fourier transform of the random variable over the domain $[0, T]$ is defined by

$$\mathscr{F}_T[\Phi_K](\omega) = \frac{1}{\sqrt{T}} \int_0^T \mathrm{d}t \, \exp(-i\omega t) \Phi_K(t). \qquad (A4)$$

Here, $\omega = 2\pi f$ is the angular frequency. Analytical functions that fall sufficiently rapid to zero, such as the pulse function ϕ, have the Fourier transform

$$\mathscr{F}[\phi](\vartheta) = \int_{-\infty}^{\infty} \mathrm{d}\theta \, \exp(-i\theta\vartheta) \phi(\theta) \qquad (A5)$$

and the inverse transform

$$\phi(\theta) = \mathscr{F}^{-1}[\mathscr{F}[\phi](\vartheta)](\theta) = \frac{1}{2\pi} \int_{-\infty}^{\infty} \mathrm{d}\vartheta \, \exp(i\theta\vartheta) \mathscr{F}[\phi](\vartheta). \qquad (A6)$$

Note that, here, θ and ϑ are non-dimensional variables, as opposed to t and ω.

Neglecting end effects in by assuming $T/\tau_\mathrm{d} \gg 1$, the frequency power spectral density of the stationary process Φ_K is found to be the product of the power of the pulse function and the power of the forcing,[114]

$$\mathscr{S}_\Phi(\omega) = |\mathscr{F}[\phi](\tau_\mathrm{d}\omega)|^2 \lim_{T \to \infty} \left\langle \left|\mathscr{F}_T\left[F_K\left(\frac{t}{\tau_\mathrm{d}}\right)\right](\omega)\right|^2 \right\rangle, \qquad (A7)$$

which is independent of K since the average is over all random variables. The frequency power spectrum for the forcing F_K will now be calculated for the case of periodic pulses.

The marginal probability density function for the pulse arrival times when these are periodic with period τ_p and starting point s, assuming that the starting time s is known, is

$$P_{t_k}(t_k|s) = \delta(t_k - \tau_\mathrm{p}k - s). \qquad (A8)$$

Since each arrival is deterministic, the joint distribution of all arrivals with known starting point is the product of the marginal distributions,

$$P_{t_1,\ldots,t_K}(t_1,\ldots,t_K|s) = \prod_{k=1}^{K} \delta(t_k - \tau_\mathrm{p}k - s). \qquad (A9)$$

To account for the fact that the periodicity but not the actual arrival time is known, the starting point is randomly and uniformly chosen in the interval $[0, \tau_\mathrm{p}]$,

$$P_s(s) = \begin{cases} \tau_\mathrm{p}^{-1}, & 0 < s < \tau_\mathrm{p} \\ 0, & \text{else.} \end{cases} \qquad (A10)$$

The Fourier transform of the forcing is

$$\mathscr{F}_T\left[F_K\left(\frac{t}{\tau_\mathrm{d}}\right)\right](\omega) = \frac{\tau_\mathrm{d}}{\sqrt{T}} \sum_{k=1}^{K} A_k \exp(-i\omega t_k). \qquad (A11)$$

Multiplying this expression with its complex conjugate and averaging over all random variables give after some calculations, the frequency power spectrum of the forcing,

$$\lim_{T \to \infty} \langle |\mathscr{F}_T[F_K](\omega)^2| \rangle = \frac{\tau_\mathrm{d}^2}{\tau_\mathrm{p}} A_\mathrm{rms}^2 + \frac{\tau_\mathrm{d}^2}{\tau_\mathrm{p}} \langle A \rangle^2 2\pi \sum_{n=-\infty}^{\infty} \delta(\tau_\mathrm{p}\omega - 2\pi n). \qquad (A12)$$

According to Eq. (A7), this is to be multiplied by the spectrum of the pulse function. Thus, the frequency power spectral density for a superposition of periodic pulses with fixed shape and duration is given by the sum of the spectrum of the pulse function (due to a random distribution of pulse amplitudes and represented by the term proportional to A_rms^2 in the above equation) and the spectrum of the pulse function multiplied by a uniform delta pulse train, also known as a Dirac comb (represented by the last term in the above equation proportional to $\langle A \rangle^2$, which vanishes for a symmetric amplitude distribution).

DATA AVAILABILITY

The data that support the findings of this study are available from the corresponding author upon reasonable request.

REFERENCES

[1] F. H. Busse, "Non-linear properties of thermal convection," Rep. Prog. Phys. **41**, 1929 (1978).
[2] E. D. Siggia, "High Rayleigh number convection," Annu. Rev. Fluid Mech. **26**, 137 (1994).
[3] E. Bodenschatz, W. Pesch, and G. Ahlers, "Recent developments in Rayleigh-Bénard convection," Annu. Rev. Fluid Mech. **32**, 709 (2000).
[4] L. P. Kadanoff, "Turbulent heat flow: Structures and scaling," Phys. Today **54**(8), 34 (2001).
[5] G. Ahlers, S. Grossmann, and D. Lohse, "Heat transfer and large scale dynamics in turbulent Rayleigh-Bénard convection," Rev. Mod. Phys. **81**, 503 (2009).
[6] M. K. Verma, *Physics of Buoyant Flows: From Instabilities to Turbulence* (World Scientific, 2018).
[7] P. Atten, J. C. Lacroix, and B. Malraison, "Chaotic motion in a Coulomb force driven instability: Large aspect ratio experiments," Phys. Lett. A **79**, 255 (1980).
[8] D. Farmer, J. Crutchfield, H. Froehling, N. Packard, and R. Shaw, "Power spectra and mixing properties of strange attractors," Ann. New York Acad. Sci. **357**, 453 (1980).
[9] U. Frisch and R. Morf, "Intermittency in nonlinear dynamics and singularities at complex times," Phys. Rev. A **23**, 2673 (1981).

[10]H. S. Greenside, G. Ahlers, P. C. Hohenberg, and R. W. Walden, "A simple stochastic model for the onset of turbulence in Rayleigh-Bénard convection," Physica D 5, 322 (1982).

[11] J. D. Farmer, "Chaotic attractors of an infinite-dimensional dynamical system," Physica D 4, 366 (1982).

[12] A. Libchaber, S. Fauve, and C. Laroche, "Two-parameter study of the routes to chaos," Physica D 7, 73 (1983).

[13] A. Brandstater and H. L. Swinney, "Strange attractors in weakly turbulent Couette-Taylor flow," Phys. Rev. A 35, 2207 (1987).

[14]D. Sigeti and W. Horsthemke, "High-frequency power spectra for systems subject to noise," Phys. Rev. A 35, 2276 (1987).

[15] E. F. Stone, "Power spectra of the stochastically forced Duffing oscillator," Phys. Lett. A 148, 434 (1990).

[16]C. L. Streett and M. Y. Hussaini, "A numerical simulation of the appearance of chaos in finite-length Taylor-Couette flow," Appl. Numer. Math. 7, 41 (1991).

[17]B. Mensour and A. Longtin, "Power spectra and dynamical invariants for delay-differential and difference equations," Physica D 113, 1 (1998).

[18]M. R. Paul, M. C. Cross, P. F. Fischer, and H. S. Greenside, "Power-law behavior of power spectra in low Prandtl number Rayleigh-Bénard convection," Phys. Rev. Lett. 87, 154501 (2001).

[19]L. A. Safonov, E. Tomer, V. V. Strygin, Y. Ashkenazy, and S. Havlin, "Multifractal chaotic attractors in a system of delay-differential equations modeling road traffic," Chaos 12, 1006 (2002).

[20]V. Schenzinger and S. M. Osprey, "Interpreting the nature of Northern and Southern Annular Mode variability in CMIP5 Models," J. Geophys. Res. Atmos. 120, 11203, https://doi.org/10.1002/2014jd022989 (2015).

[21] A. M. Reynolds, F. Bartumeus, A. Kölzsch, and J. van de Koppel, "Signatures of chaos in animal search patterns," Sci. Rep. 6, 23492 (2015).

[22]S. Paul, P. K. Mishra, M. K. Verma and K. Kumar, "Order and chaos in two-dimensional Rayleigh-Bénard convection," arXiv:0904.2917 [physics.flu-dyn].

[23] D. E. Sigeti, "Exponential decay of power spectra at high frequency and positive Lyapunov exponents," Physica D 82, 136 (1995).

[24]D. E. Sigeti, "Survival of deterministic dynamics in the presence of noise and the exponential decay of power spectra at high frequency," Phys. Rev. E 52, 2443 (1995).

[25]D. S. Broomhead and G. P. King, "Extracting qualitative dynamics from experimental data," Physica D 20, 2017 (1986).

[26]S. M. Osprey and M. H. P. Ambaum, "Evidence for the chaotic origin of northern annular mode variability," Geopyhs. Res. Lett. 38, L15702, https://doi.org/10.1029/2011gl048181 (2011).

[27]C. L. E. Franzke, S. M. Osprey, P. Davini, and N. W. Watkins, "A dynamical systems explanation of the Hurst effect and atmospheric low-frequency variability," Sci. Rep. 5, 9068 (2015).

[28]S. Paul, P. Wahi, and M. K. Verma, "Bifurcations and chaos in large-Prandtl number Rayleigh-Bénard convection," Int. J. Nonlinear Mech. 46, 772 (2011).

[29]N. Ohtomo, K. Tokiwano, Y. Tanaka, A. Sumi, S. Terachi, and H. Konno, "Exponential characteristics of power spectral densities caused by chaotic phenomena," J. Phys. Soc. Jpn. 64, 1104 (1995).

[30]J. E. Maggs and G. J. Morales, "Origin of Lorentzian pulses in deterministic chaos," Phys. Rev. E 86, 015401 (2012).

[31] D. C. Pace, M. Shi, J. E. Maggs, G. J. Morales, and T. A. Carter, "Exponential frequency spectrum and Lorentzian pulses in magnetized plasmas," Phys. Plasmas 15, 122304 (2008).

[32]D. C. Pace, M. Shi, J. E. Maggs, G. J. Morales, and T. A. Carter, "Exponential frequency spectrum in magnetized plasmas," Phys. Rev. Lett. 101, 085001 (2008).

[33]G. Hornung, B. Nold, J. E. Maggs, G. J. Morales, M. Ramisch, and U. Stroth, "Observation of exponential spectra and Lorentzian pulses in the TJ-K stellarator," Phys. Plasmas 18, 082303 (2011).

[34]J. E. Maggs and G. J. Morales, "Generality of deterministic chaos, exponential spectra, and Lorentzian pulses in magnetically confined plasmas," Phys. Rev. Lett. 107, 185003 (2011).

[35]J. E. Maggs and G. J. Morales, "Exponential power spectra, deterministic chaos and Lorentzian pulses in plasma edge dynamics," Plasma Phys. Contr. Fusion 54, 124041 (2012).

[36]B. Ph. van Milligen, R. Sánchez, and C. Hidalgo, "Relevance of uncorrelated Lorentzian pulses for the interpretation of turbulence in the edge of magnetically confined toroidal plasmas," Phys. Rev. Lett. 109, 105001 (2012).

[37]J. E. Maggs and G. J. Morales, "Permutation entropy analysis of temperature fluctuations from a basic electron heat transport experiment," Plasma Phys. Controlled Fusion 55, 085015 (2013).

[38]Z. Zhu, A. E. White, T. A. Carter, S. G. Baek, and J. L. Terry, "Chaotic edge density fluctuations in the Alcator C-Mod tokamak," Phys. Plasmas 24, 042301 (2017).

[39]O. E. Garcia and A. Theodorsen, "Power law spectra and intermittent fluctuations due to uncorrelated Lorentzian pulses," Phys. Plasmas 24, 020704 (2018).

[40]O. E. Garcia and A. Theodorsen, "Skewed Lorentzian pulses and exponential frequency power spectra," Phys. Plasmas 25, 014503 (2018).

[41] O. E. Garcia and A. Theodorsen, "Intermittent fluctuations due to uncorrelated Lorentzian pulses," Phys. Plasmas 25, 014506 (2018).

[42]G. J. Morales, "Investigation of a chaotic thermostat," Phys. Rev. E 97, 032203 (2018).

[43]G. J. Morales, "Two-dimensional chaotic thermostat and behavior of a thermalized charge in a weak magnetic field," Phys. Rev. E 99, 062218 (2019).

[44]F. H. Busse, "Generation of mean flows by thermal convection," Physica D 9, 287 (1983).

[45]L. N. Howard and R. Krishnamurti, "Large-scale flow in turbulent convection: A mathematical model," J. Fluid Mech. 170, 385 (1986).

[46]J. F. Drake, J. M. Finn, P. Guzdar, V. Shapiro, V. Shevchenko, F. Waelbroeck, A. B. Hassam, C. S. Liu, and R. Sagdeev, "Peeling of convection cells and the generation of sheared flow," Phys. Fluids B 4, 488 (1992).

[47]J. M. Finn, J. F. Drake, and P. N. Guzdar, "Instability of fluid vortices and generation of sheared flow," Phys. Fluids B 4, 2758 (1992).

[48]A. M. Rucklidge and P. C. Matthews, "Analysis of the shearing instability in nonlinear convection and magnetoconvection," Nonlinearity 9, 311 (1996).

[49]J. G. Fitzgerald and B. F. Farrell, "Mechanisms of mean flow formation and suppression in two-dimensional Rayleigh-Bénard convection," Phys. Fluids 26, 054104 (2014).

[50]O. Pogutse, W. Kerner, V. Gribkov, S. Bazdenkov, and M. Osipenko, "The resistive interchange convection in the edge of tokamak plasmas," Plasma Phys. Controlled Fusion 36, 1963 (1994).

[51] H. Sugama and W. Horton, "L-H confinement mode dynamics in three-dimensional state space," Plasma Phys. Controlled Fusion 37, 345 (1995).

[52] P. Beyer and K. H. Spatschek, "Center manifold theory for the dynamics of the L-H-transition," Phys. Plasmas 3, 995 (1996).

[53]W. Horton, G. Hu, and G. Laval, "Turbulent transport in mixed states of convective cells and sheared flows," Phys. Plasmas 3, 2912 (1996).

[54]M. Berning and K. H. Spatschek, "Bifurcations and transport barriers in the resistive-g paradigm," Phys. Rev. E 62, 1162 (2000).

[55]K. B. Hermiz, P. N. Guzdar, and J. M. Finn, "Improved low-order model for shear flow driven by Rayleigh-Bénard convection," Phys. Rev. E 51, 325 (1995).

[56]J. Prat, J. M. Massaguer, and I. Mercader, "Large-scale flows and resonances in 2-D thermal convection," Phys. Fluids 7, 121 (1995).

[57]J. M. Finn, "Nonlinear interaction of Rayleigh-Taylor and shear instabilities," Phys. Fluids B 5, 415 (1993).

[58]J. M. Finn and K. Hermiz, "The role of self-consistent Lagrangian chaos in Bénard convection in an annulus," Phys. Fluids B 5, 3897 (1993).

[59]A. Takayama, T. Unemura, and M. Wakatani, "Comparison of Lorenz type and plasma fluid models for nonlinear-interchange-mode generation of shear flow," Plasma Phys. Controlled Fusion 40, 775 (1998).

[60]O. E. Garcia, N. H. Bian, J.-V. Paulsen, S. Benkadda, and K. Rypdal, "Confinement and bursty transport in a flux-driven convection model with sheared flows," Plasma Phys. Controlled Fusion 45, 919 (2003).

[61] O. E. Garcia and N. H. Bian, "Bursting and large-scale intermittency in turbulent convection with differential rotation," Phys. Rev. E 68, 047301 (2003).

[62]O. E. Garcia, N. H. Bian, V. Naulin, A. H. Nielsen, and J. J. Rasmussen, "Two-dimensional convection and interchange motions in fluids and magnetized plasmas," Phys. Scr. T122, 104 (2006).

[63]N. Bian, S. Benkadda, O. E. Garcia, J.-V. Paulsen, and X. Garbet, "The quasilinear behavior of convective turbulence with sheared flows," Phys. Plasmas **10**, 1382 (2003).

[64]N. H. Brummell and J. E. Hart, "High Rayleigh number β-convection," Geophys. Astrophys. Fluid Dyn. **68**, 85 (1993).

[65]F. H. Busse and R. M. Clever, "Bursts in inclined layer convection," Phys. Fluids **12**, 2137 (2000).

[66]E. Grote, F. H. Busse, and A. Tilgner, "Regular and chaotic spherical dynamos," Phys. Earth Planet. Inter. **117**, 259 (2000).

[67]U. R. Christensen, "Zonal flow driven by deep convection in the major planets," Geopyhs. Res. Lett. **28**, 2553, https://doi.org/10.1029/2000gl012643 (2001).

[68]J. M. Aurnou and P. L. Olson, "Strong zonal winds from thermal convection in a rotating spherical shell," Geopyhs. Res. Lett. **28**, 2557, https://doi.org/10.1029/2000gl012474 (2001).

[69]F. H. Busse, "Convective flows in rapidly rotating spheres and their dynamo action," Phys. Fluids **14**, 1301 (2002).

[70]U. R. Christensen, "Zonal flow driven by strongly supercritical convection in rotating spherical shells," J. Fluid Mech. **470**, 115 (2002).

[71]E. Grote and F. H. Busse, "Dynamics of convection and dynamos in rotating spherical fluid shells," Fluid Dyn. Res. **28**, 349 (2001).

[72]V. Morin and E. Dormy, "Time dependent β-convection in rapidly rotating spherical shells," Phys. Fluids **16**, 1603 (2004).

[73]J.-J. Tau and W.-C. Tan, "Relaxation oscillation of thermal convection in rotating cylindrical annulus," Chin. Phys. Lett. **28**, 034706 (2011).

[74]R. J. Teed, C. A. Jones, and R. Hollerbach, "On the necessary conditions for bursts of convection within the rapidly rotating cylindrical annulus," Phys. Fluids **24**, 066604 (2012).

[75]A. Takayama, M. Wakatani, and H. Sugama, "Suppression of nonlinear interchange mode by zonal counterstreaming flow generation," Phys. Plasmas **3**, 3 (1996).

[76]P. N. Guzdar and A. B. Hassam, "A self-consistent model for low-high transitions in tokamaks," Phys. Plasmas **3**, 3701 (1996).

[77]Z. Lin, T. S. Hahm, W. W. Lee, W. M. Tang, and P. H. Diamond, "Effects of collisional zonal flow damping on turbulent transport," Phys. Rev. Lett. **83**, 3645 (1999).

[78]Z. Lin, T. S. Hahm, W. W. Lee, W. M. Tang, and R. B. White, "Gyrokinetic simulations in general geometry and applications to collisional damping of zonal flows," Phys. Plasmas **7**, 1857 (2000).

[79]M. A. Malkov, P. H. Diamond, and M. N. Rosenbluth, "On the nature of bursting in transport and turbulence in drift wave-zonal flow systems," Phys. Plasmas **8**, 5073 (2001).

[80]K. Takeda, S. Hamaguchi, and M. Wakatani, "ELM-like behaviour generated by nonlinear ion-temperature-gradient-driven mode," Plasma Phys. Controlled Fusion **44**, A487 (2002).

[81]V. Naulin, J. Nycander, and J. J. Rasmussen, "Transport barriers and edge localized modes in a plasma model with turbulent equipartition profiles," Phys. Plasmas **10**, 1075 (2003).

[82]G. Manfredi and C. M. Roach, "Bursting events in zonal flow-drift wave turbulence," Phys. Plasmas **10**, 2824 (2003).

[83]O. E. Garcia, V. Naulin, A. H. Nielsen, and J. Juul Rasmussen, "Turbulence and intermittent transport at the boundary of magnetized plasmas," Phys. Plasmas **12**, 062309 (2005).

[84]P. Beyer, S. Benkadda, G. Fuhr-Chaudier, X. Garbet, Ph. Ghendrih, and Y. Sarazin, "Nonlinear dynamics of transport barrier relaxations in Tokamak edge plasmas," Phys. Rev. Lett. **94**, 105001 (2005).

[85]O. E. Garcia, V. Naulin, A. H. Nielsen, and J. J. Rasmussen, "Turbulence simulations of blob formation and radial propagation in toroidally magnetized plasmas," Phys. Scr. **T122**, 89 (2006).

[86]R. G. Kleva and P. N. Guzdar, "Zonal flow sawteeth and the time period between edge-localized transport bursts in tokamaks," Phys. Plasmas **14**, 012303 (2007).

[87]N. H. Bian and O. E. Garcia, "Confinement and dynamical regulation in two-dimensional convective turbulence," Phys. Plasmas **10**, 4696 (2003).

[88]O. E. Garcia and N. H. Bian, "Shear dispersion and turbulence decorrelation by differential rotation," Phys. Plasmas **12**, 014503 (2005).

[89]N. H. Bian, "On-off intermittent regulation of plasma turbulence," Phys. Plasmas **17**, 044501 (2010).

[90]H. Zhu, S. C. Chapman, and R. O. Dendy, "Robustness of predator-prey models for confinement regime transitions in fusion plasmas," Phys. Plasmas **20**, 042302 (2013).

[91]F. Heslot, B. Castaing, and A. Libchaber, "Transitions to turbulence in helium gas," Phys. Lett. A **36**, 5870 (1987).

[92]B. Castaing, G. Gunaratne, F. Heslot, L. Kadanoff, A. Libchaber, S. Thomae, X.-Z. Wu, S. Zaleski, and G. Zanetti, "Scaling of hard thermal turbulence in Rayleigh-Bénard convection," J. Fluid Mech. **204**, 1 (1989).

[93]M. Sano, X. Z. Wu, and A. Libchaber, "Turbulence in helium-gas free convection," Phys. Lett. A **40**, 6421 (1989).

[94]E. E. DeLuca, J. Werne, R. Rosner, and F. Cattaneo, "Numerical simulations of soft and hard turbulence: Preliminary results for two-dimensional convection," Phys. Rev. Lett. **64**, 2370 (1990).

[95]F. Massaioli, R. Benzi, and S. Succi, "Exponential tails in two-dimensional Rayleigh-Bénard convection," Europhys. Lett. **21**, 305 (1993).

[96]J. Werne, "Structure of hard-turbulent convection in two dimensions: Numerical evidence," Phys. Rev. E **48**, 1020 (1993).

[97]K. Julien, S. Legg, J. McWilliams, and J. Werne, "Hard turbulence in rotating Rayleigh-Bénard convection," Phys. Rev. E **53**, R5557 (1996).

[98]B. I. Shraiman and E. D. Siggia, "Heat transport in high-Rayleigh-number convection," Phys. Rev. A **42**, 3650 (1990).

[99]S. Cioni, S. Ciliberto, and J. Sommeria, "Strongly turbulent Rayleigh-Bénard convection in mercury: Comparison with results at moderate Prandtl number," J. Fluid Mech. **335**, 111 (1997).

[100]J. J. Niemela, L. Skrbek, K. R. Sreenivasan, and R. J. Donnelly, "Turbulent convection at very high Rayleigh numbers," Nature **404**, 837 (2000).

[101]R. Verzicco and K. R. Sreenivasan, "A comparison of turbulent thermal convection between conditions of constant temperature and constant heat flux," J. Fluid Mech. **595**, 203 (2008).

[102]H. Johnston and C. R. Doering, "Comparison of turbulent thermal convection between conditions of constant temperature and constant flux," Phys. Rev. Lett. **102**, 064501 (2009).

[103]S.-D. Huang, F. Wang, H.-D. Xi, and K.-Q. Xia, "Comparative experimental study of fixed temperature and fixed heat flux boundary conditions in turbulent thermal convection," Phys. Rev. Lett. **115**, 154502 (2015).

[104]V. Naulin and A. H. Nielsen, "Accuracy of spectral and finite difference schemes in 2D advection problems," SIAM J. Sci. Comput. U. S. A. **25**, 104 (2003).

[105]O. E. Garcia, V. Naulin, A. H. Nielsen, and J. Juul Rasmussen, "Computations of intermittent transport in scrape-off layer plasmas," Phys. Rev. Lett. **92**, 165003 (2004).

[106]S. O. Rice, "Mathematical analysis of random noise," Bell Syst. Tech. J. **23**, 282 (1944).

[107]E. Daly and A. Porporato, "Effect of different jump distributions on the dynamics of jump processes," Phys. Rev. E **81**, 061133 (2010).

[108]O. E. Garcia, "Stochastic modeling of intermittent scrape-off layer plasma fluctuations," Phys. Rev. Lett. **108**, 265001 (2012).

[109]R. Kube and O. E. Garcia, "Convergence of statistical moments of particle density time series in scrape-off layer plasmas," Phys. Plasmas **22**, 012502 (2015).

[110]A. S. Bergsaker, Å. Fredriksen, H. L. Pécseli, and J. K. Trulsen, "Models for the probability densities of the turbulent plasma flux in magnetized plasmas," Phys. Scr. **90**, 108005 (2015).

[111]A. Theodorsen and O. E. Garcia, "Level crossings, excess times, and transient plasma-wall interactions in fusion plasmas," Phys. Plasmas **23**, 040702 (2016).

[112]O. E. Garcia, R. Kube, A. Theodorsen, and H. L. Pécseli, "Stochastic modelling of intermittent fluctuations in the scrape-off layer: Correlations, distributions, level crossings, and moment estimation," Phys. Plasmas **23**, 052308 (2016).

[113]F. Militello and J. T. Omotani, "Scrape off layer profiles interpreted with filament dynamics," Nucl. Fusion **56**, 104004 (2016).

[114]A. Theodorsen, O. E. Garcia, and M. Rypdal, "Statistical properties of a filtered Poisson process with additive random noise: Distributions, correlations and moment estimation," Phys. Scr. **92**, 054002 (2017).

[115]O. E. Garcia and A. Theodorsen, "Auto-correlation function and frequency spectrum due to a super-position of uncorrelated exponential pulses," Phys. Plasmas **24**, 032309 (2017).

[116]A. Theodorsen and O. E. Garcia, "Probability distribution functions for intermittent scrape-off layer plasma fluctuations," Plasma Phys. Controlled Fusion **60**, 034006 (2018).

[117]A. Theodorsen and O. E. Garcia, "Level crossings and excess times due to a superposition of uncorrelated exponential pulses," Phys. Rev. E **97**, 012110 (2018).

[118]A. Theodorsen, O. E. Garcia, R. Kube, B. LaBombard, and J. L. Terry, "Universality of Poisson-driven plasma fluctuations in the Alcator C-Mod scrape-off layer," Phys. Plasmas **25**, 122309 (2018).

[119]W. H. Richardson, "Bayesian-based iterative method of image restoration," J. Opt. Soc. Am. **62**, 55 (1972).

[120]L. B. Lucy, "An iterative technique for the rectification of observed distributions," Astron. J. **79**, 745 (1974).

[121]M. E. Daube-Witherspoon and G. Muehllehner, "An iterative image space reconstruction algorithm suitable for volume ECT," IEEE Trans. Med. Imaging **5**, 61 (1986).

[122]F. Dell'Acqua, G. Rizzo, P. Scifo, R. A. Clarke, G. Scotti, and F. Fazio, "A model-based deconvolution approach to solve fiber crossing in diffusion-weighted MR imaging," IEEE Trans. Biomed. Eng. **54**, 462 (2007).

[123]Y.-W. Tai, P. Tan, and M. S. Brown, "Richardson-Lucy deblurring for scenes under a projective motion path," IEEE Trans. Pattern Anal. Mach. Intell. **33**, 1603 (2011).